

General transmission conditions for thin elasto-plastic pressure-dependent interphase between dissimilar materials

M. SONATO¹, A. PICCOLROAZ*¹, W. MISZURIS², AND G. MISHURIS²

¹*Department of Civil, Environmental and Mechanical Engineering, University of Trento, Italy*

²*Department of Mathematics, Aberystwyth University, Aberystwyth, U.K.*

Abstract

We consider a thin soft adhesive interphase between dissimilar elastic media. The material of the intermediate layer is modelled by elasto-plastic pressure-sensitive constitutive law. An asymptotic procedure, together with a novel formulation of the deformation theory of plasticity for pressure-sensitive materials, is used in order to derive nonlinear transmission conditions for the corresponding imperfect zero-thickness interface. A FEM analysis of the original three-phase structure is performed to validate the transmission conditions for the simplified bimaterial structure.

Keywords: Adhesive joint; Pressure-sensitive deformation theory; Imperfect interface; Nonlinear transmission conditions

1 Introduction

Adhesive joints are widely used in structural engineering applications involving composite materials, such as marine [1], aerospace [2] and automotive [3] structures. In these structures, polymeric adhesives are used to join different materials such as plastics, metals, fibre reinforced composites and others.

Early models of adhesive joints tended to assume that the adhesive behaves as a linear-elastic solid [4, 5]. However, many adhesives (e.g. rubber modified epoxies) exhibit large plastic strains before failure [6]. A number of yield criteria have been proposed to model the plastic behaviour of polymers. Among these, the Tresca and von Mises criteria, originally developed to describe the yield behaviour of metals, have been also used. However, these criteria cannot accurately predict the behaviour of polymeric adhesive specimens under multiaxial loading, as yielding in these materials is sensitive to hydrostatic as well as the deviatoric stress [7, 8]. As a consequence, pressure-dependent plasticity theory is more appropriate in this case. In this context, the Drucker-Prager yield criterion is widely used for polymeric materials.

*Corresponding author: e-mail: roaz@ing.unitn.it; phone: +39 0461 282583.

The numerical FE modelling of thin adhesive interphases is complicated by the very large aspect ratio of the intermediate layer, which requires extremely refined meshes. Alternatively, the so-called imperfect interface approach can be adopted. It consists of replacing the actual thin interphase between the two adherents by a zero thickness imperfect interface. The interface is supplied with special transmission conditions, which incorporate information about geometrical and mechanical properties of the original thin interphase.

Although imperfect transmission conditions for elastic interphases have been intensively investigated [9–12], analytical results for elastoplastic adhesive interphase are very scarce and mainly limited to rigid adherents and pressure-independent plasticity [13, 14].

In this paper, nonlinear transmission conditions for a soft elasto-plastic *pressure-dependent* interphase are derived by asymptotic techniques. The interphase material is described by a novel formulation of the deformation theory for pressure-dependent media. Early models of pressure-dependent deformation theory can be found in [15] and [16]. However, the model proposed by [15] only accounts for elastic and plastic branches separately, i.e. the yield condition is not incorporated into the generalized constitutive parameters. On the other hand, the model proposed in [16] applies only to a few specific loading paths. To overcome these limitations, the classical Hencky deformation theory is generalized in Section 3 to the case of pressure-sensitive materials by including the dependence of inelastic deformation on the first stress invariant, in the spirit suggested by Chen [17] and Lubarda [18]. The general theory is then specialized to the the case of Drucker-Prager model with associated flow rule and isotropic linear hardening.

The transmission conditions are validated by numerical examples based on accurate finite element simulations. The accuracy and efficiency of the proposed approach prove to be very high for different monotonic loading conditions.

2 Problem formulation and transmission conditions for elasto-plastic pressure-dependent interphases

Consider a structure composed by two dissimilar elastic materials joined together by a thin adhesive interphase, see Fig. 1. The thickness of the interphase is small in comparison with the characteristic size of the body: $h = \epsilon h_* \ll L$, $h_* \sim L$. Here ϵ is a small positive parameter, $\epsilon \ll 1$.

The adhesive material is assumed to be soft in comparison with the two adherents and may exhibit a very general nonlinear constitutive behaviour, including compressible plastic deformations, the only assumption being that the material is isotropic.

Adopting the deformation theory of plasticity, the constitutive laws of the interphase in the plastic regime will be described in terms of nonlinear elasticity as

$$\sigma_{ij} = \tilde{\lambda} \varepsilon_{kk} \delta_{ij} + 2\tilde{\mu} \varepsilon_{ij}, \quad (1)$$

where the generalized Lamé parameters are functions depending on the deformation within the interphase

$$\tilde{\lambda} = \tilde{\lambda}(J_1^\varepsilon, J_2^\varepsilon), \quad \tilde{\mu} = \tilde{\mu}(J_1^\varepsilon, J_2^\varepsilon). \quad (2)$$

Note that, due to the isotropy assumption, the dependence is written in terms of the two invariants

$$J_1^\varepsilon = \varepsilon_{kk}, \quad J_2^\varepsilon = \frac{1}{2} e_{ij} e_{ij}, \quad (3)$$

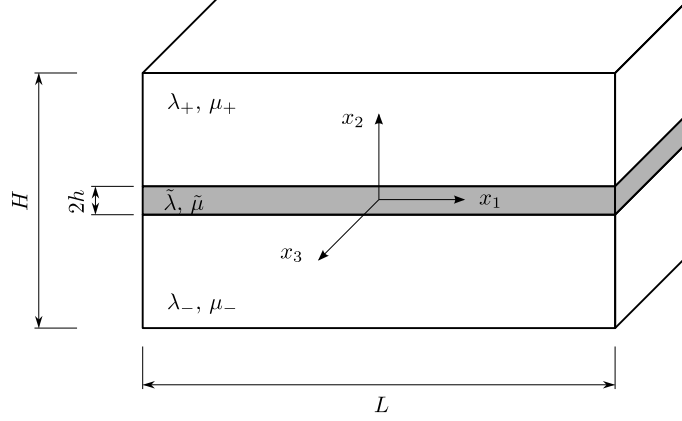


Figure 1: Bimaterial structure with thin soft adhesive joint.

where e_{ij} denotes the deviatoric part of the strain tensor. For the sake of keeping the analysis simple, the dependence on the third invariant is omitted. However, if necessary, the model can be generalized to include the effect of all invariants.

In the elastic regime, the elastic constants are assumed to be constant

$$\lambda = \epsilon\lambda_0, \quad \mu = \epsilon\mu_0, \quad (4)$$

where the elastic parameters λ_0, μ_0 are comparable with those of the adherent materials, λ_{\pm}, μ_{\pm} .

We assume in our analysis that, for any admissible deformation of the material within the interphase, there exists a constant parameter ν_* such that

$$0 \leq \tilde{\nu}(J_1^e, J_2^e) \leq \nu_* < 1/2, \quad (5)$$

where $\tilde{\nu}(J_1^e, J_2^e)$ is the generalized Poisson's ratio

$$\tilde{\nu}(J_1^e, J_2^e) = \frac{\tilde{\lambda}(J_1^e, J_2^e)}{2[\tilde{\lambda}(J_1^e, J_2^e) + \tilde{\mu}(J_1^e, J_2^e)]}. \quad (6)$$

Under such assumption, the following two imperfect transmission conditions linking the values from different parts of the interphase are asymptotically satisfied, see [16]

$$\llbracket \mathbf{t}_2 \rrbracket(x_1, x_3) = 0, \quad (7)$$

and

$$\mathbf{t}_2(x_1, x_3) = \frac{1}{2h} \mathbf{A}(x_1, x_3) \llbracket \mathbf{u} \rrbracket(x_1, x_3), \quad (8)$$

where $\mathbf{t}_2 = [\sigma_{21}, \sigma_{22}, \sigma_{23}]^T$ is the traction on the interphase surfaces, $\mathbf{u} = [u_1, u_2, u_3]^T$ is the displacement vector, and the jump of a function f across the interphase is denoted by $\llbracket f \rrbracket = f(x_2 = h) - f(x_2 = -h)$, and the tensor \mathbf{A} is given by

$$\mathbf{A} = \begin{pmatrix} \tilde{\mu} & 0 & 0 \\ 0 & \tilde{\lambda} + 2\tilde{\mu} & 0 \\ 0 & 0 & \tilde{\mu} \end{pmatrix}. \quad (9)$$

The transmission conditions (7) and (8) are valid under the following ellipticity conditions

$$0 < \tilde{\mu} < \epsilon\mu_*, \quad 0 < \tilde{\lambda} + 2\tilde{\mu} < \epsilon\Lambda_*, \quad (10)$$

where μ_* and Λ_* are constants comparable in values with those of the adherent materials. In fact, we can take $\mu_* = \mu_0$ and $\Lambda_* = \lambda_0 + 2\mu_0$.

The asymptotic procedure allows us also to estimate the components of the strain tensor, which to the leading order $O(\epsilon^{-1})$ read

$$\varepsilon_{ij} = O(1), \quad \varepsilon_{i2} = \frac{1}{2} \frac{\partial u_i}{\partial x_2} + O(1), \quad i, j = 1, 3, \quad \varepsilon_{22} = \frac{\partial u_2}{\partial x_2}. \quad (11)$$

By application of the generalized Hooke's law (1), we obtain the following relationships

$$\varepsilon_{i2} = \frac{\sigma_{i2}}{2\tilde{\mu}}, \quad i, j = 1, 3, \quad \varepsilon_{22} = \frac{\sigma_{22}}{\tilde{\lambda} + 2\tilde{\mu}}, \quad (12)$$

Finally, the leading terms of the strain tensor invariants can be calculated as

$$J_1^\varepsilon = \varepsilon_{22} = \frac{\sigma_{22}}{\tilde{\lambda} + 2\tilde{\mu}}, \quad (13)$$

$$J_2^e = \frac{1}{3}\varepsilon_{22}^2 + \varepsilon_{12}^2 + \varepsilon_{23}^2 = \frac{1}{3} \frac{\sigma_{22}^2}{(\tilde{\lambda} + 2\tilde{\mu})^2} + \frac{1}{4} \frac{\sigma_{12}^2}{\tilde{\mu}^2} + \frac{1}{4} \frac{\sigma_{23}^2}{\tilde{\mu}^2}. \quad (14)$$

Note that the material functions $\tilde{\lambda}$ and $\tilde{\mu}$, at this point, are not specified and should be defined depending on the particular elasto-plastic model adopted for the interphase material. However, all the stress components σ_{i2} of the traction vector \mathbf{t}_2 as well as the components of the strain tensor ε_{ij} in their leading terms are functions only of the space variables x_1 and x_3 . This immediately implies that, in the case under consideration, the strain invariants are also functions of those two variables,

$$J_1^\varepsilon = J_1^\varepsilon(x_1, x_3), \quad J_2^e = J_2^e(x_1, x_3). \quad (15)$$

The transmission conditions (8) are then used to write the strain invariants (13) and (14) in terms of components of displacement jump

$$J_1^\varepsilon = \frac{1}{2h} \llbracket u_2 \rrbracket, \quad (16)$$

$$J_2^e = \frac{1}{12h^2} \llbracket u_2 \rrbracket^2 + \frac{1}{16h^2} \llbracket u_1 \rrbracket^2 + \frac{1}{16h^2} \llbracket u_3 \rrbracket^2. \quad (17)$$

This allows us to formulate the nonlinear transmission conditions for a thin soft nonlinear interphase in their final form

$$\llbracket \mathbf{t}_2 \rrbracket = 0, \quad \mathbf{t}_2 = \frac{1}{2h} \mathbf{A}(\llbracket \mathbf{u} \rrbracket) \llbracket \mathbf{u} \rrbracket, \quad (18)$$

where the matrix-function \mathbf{A} is explicitly defined by $\mathbf{A}(\llbracket \mathbf{u} \rrbracket) = \mathbf{A}(\tilde{\lambda}(J_1^\varepsilon, J_2^e), \tilde{\mu}(J_1^\varepsilon, J_2^e))$ and the relationships (16) and (17).

Let us recall that the assumptions (10) should be satisfied to ensure the applicability of the transmission conditions. However, even if the estimates (10) cannot be checked a priori, the nonlinear transmission conditions (18) can be successfully used in the modelling. In this case, a posteriori verification of (10) will be necessary in order to confirm the validity of the final results.

Summarizing, eqs. (18) constitute the transmission conditions describing a soft imperfect interface in a bimaterial structure. These conditions allows one to replace the thin plastic interphase with an imperfect nonlinear interface (of zero thickness) and consider a simplified outer problem for the two bonded materials. The thin interphase influences the solution only via the imperfect transmission conditions which incorporates the most important information on the properties of the adhesive material and the nonlinear deformations developing within the interphase.

However, in order to use the nonlinear imperfect transmission conditions (18) one needs to define the generalized Lamé parameters (2) as functions of the strain invariants depending on the mechanical properties of the interphase material. If the parameters are constant, the conditions reduces to the thin soft elastic interphase case. In case of elasto-plastic material obeying the von Mises criterion, the analysis was presented in [14]. In the next section, we derive the proper deformation theory for a pressure-dependent plastic material, with particular reference to the Drucker-Prager criterion.

3 Pressure-dependent deformation theory

3.1 Main Assumptions

In this section, the classical J_2 deformation theory is generalized to the case of pressure-sensitive materials, so that the first invariant J_1 will also be included in the formulation. We make the following assumptions:

- The material is initially isotropic.
- The principal axes of the plastic strain tensor ε_{ij}^p are coincident with those of the stress tensor σ_{ij} .
- The plastic deviatoric strain tensor e_{ij}^p is proportional to the deviatoric stress tensor s_{ij} .

In the following, it is convenient to introduce the volumetric and deviatoric decomposition of the stress and strain tensor as:

$$\sigma_{ij} = \sigma_m \delta_{ij} + s_{ij}, \quad \sigma_m = \frac{1}{3} \sigma_{kk}, \quad (19)$$

$$\varepsilon_{ij} = \varepsilon_m \delta_{ij} + e_{ij}, \quad \varepsilon_m = \frac{1}{3} \varepsilon_{kk}, \quad (20)$$

and the additive composition of the elastic and plastic strains

$$\varepsilon_{ij} = \varepsilon_{ij}^e + \varepsilon_{ij}^p = (\varepsilon_m^e + \varepsilon_m^p) \delta_{ij} + e_{ij}^e + e_{ij}^p, \quad (21)$$

in order to derive the closed-form relationship. According to assumptions (2) and (3), the plastic strain can be written as

$$\varepsilon_{ij}^p = \phi_1 \sigma_m \delta_{ij} + \phi_2 s_{ij}, \quad (22)$$

where ϕ_1 and ϕ_2 are functions which represent the hardening behaviour of the material. In the case of plastic loading, it holds that $\phi_1 \neq 0$ and $\phi_2 > 0$, while in the case of elastic loading $\phi_1 = \phi_2 = 0$ prevails. Note that Eq. (22) can be derived following Chen's suggestions [17].

The constitutive relation between stress and elastic strain decomposed in its volumetric and deviatoric parts is given by

$$e_{ij}^e = \frac{s_{ij}}{2G}, \quad \varepsilon_m^e = \frac{\sigma_m}{3K}. \quad (23)$$

The material is assumed to be elastic compressible, so that $0 \leq \nu < 1/2$ and $K < \infty$.

Under the given assumptions, the nonlinear stress-strain law for a pressure-dependent plastic material becomes

$$\sigma_{ij} = 3\tilde{\lambda}\varepsilon_m\delta_{ij} + 2\tilde{\mu}\varepsilon_{ij}, \quad (24)$$

where the generalized Lamé's coefficients have been introduced:

$$\tilde{\lambda}(\phi_1, \phi_2) = \frac{3\nu + (\phi_2 - \phi_1)E}{3(1 + \nu + \phi_2E)(1 - 2\nu + \phi_1E)}E, \quad \tilde{\mu}(\phi_2) = \frac{E}{2(1 + \nu + \phi_2E)}, \quad (25)$$

It should be noted here that these coefficients coincide in the pure elastic regime ($\phi_1 = \phi_2 = 0$) with the elastic Lamé's coefficients. Further relationships for generalized elastic constants can be derived in the same manner:

$$\tilde{E}(\phi_1, \phi_2) = \frac{3E}{3 + (2\phi_2 + \phi_1)E}, \quad \tilde{\nu}(\phi_1, \phi_2) = \frac{3\nu + (\phi_2 - \phi_1)E}{3 + (2\phi_2 + \phi_1)E}, \quad \tilde{K}(\phi_1) = \frac{E}{3(1 - 2\nu + \phi_1E)}. \quad (26)$$

To define the functions ϕ_1 and ϕ_2 , let us consider the relationships for the first and second invariants of the strain and stress tensor, i.e.

$$J_1^{\varepsilon^p} = \varepsilon_{kk}^p, \quad J_1^\sigma = \sigma_{kk}, \quad J_2^{\varepsilon^p} = \frac{1}{2}e_{ij}^p e_{ij}^p, \quad J_2^s = \frac{1}{2}s_{ij}s_{ij}, \quad (27)$$

where the proportionality relation (22) can be used to obtain:

$$J_1^{\varepsilon^p} = 3\phi_1\sigma_m = \phi_1 J_1^\sigma, \quad J_2^{\varepsilon^p} = \frac{1}{2}\phi_2^2 s_{ij}s_{ij} = \phi_2^2 J_2^s. \quad (28)$$

Thus, the scalar functions ϕ_1 and ϕ_2 can be obtained in the case of a multiaxial stress state as

$$\phi_1 = \frac{J_1^{\varepsilon^p}}{J_1^\sigma}, \quad \phi_2 = \frac{\sqrt{J_2^{\varepsilon^p}}}{\sqrt{J_2^s}}. \quad (29)$$

In order that these relations can be used in the analysis of the thin plastic layer, the functions ϕ_1 and ϕ_2 must be defined in terms of total strain invariants. From the nonlinear elasticity relationship (24), it is noted that the first invariants of the stress tensor and the total strain tensor are linearly dependent,

$$J_1^\sigma = (3\tilde{\lambda} + 2\tilde{\mu}) J_1^\varepsilon = 3\tilde{K} J_1^\varepsilon, \quad (30)$$

whereas the second invariants of the deviatoric tensors are related by

$$\sqrt{J_2^s} = 2\tilde{\mu} \sqrt{J_2^e}. \quad (31)$$

This, in turns, allows us to evaluate the generalized material parameters as functions of the invariants

$$2\tilde{\mu} = \frac{\sqrt{J_2^s}}{\sqrt{J_2^e}}, \quad 3\tilde{K} = \frac{J_1^\sigma}{J_1^\varepsilon}. \quad (32)$$

Substituting these relations into Eqs. (25) and (26), one can define after some algebra:

$$\phi_1 = \frac{J_1^\varepsilon}{J_1^\sigma} - \frac{1-2\nu}{E}, \quad \phi_2 = \frac{\sqrt{J_2^e}}{\sqrt{J_2^s}} - \frac{1+\nu}{E}. \quad (33)$$

These relationships are more useful in the analysis than (29). This also gives the well known relationships between the invariants of the plastic strain and the total strain¹:

$$J_1^\varepsilon = J_1^{\varepsilon^p} + \frac{1-2\nu}{E} J_1^\sigma, \quad \sqrt{J_2^e} = \sqrt{J_2^{\varepsilon^p}} + \frac{1+\nu}{E} \sqrt{J_2^s}. \quad (34)$$

In the next section, we develop the deformation theory in the case of uniaxial stress state. In Section 3.3, the deformation theory is generalized to the case of general multiaxial state and Drucker-Prager material.

3.2 Uniaxial Stress Test

The uniaxial stress test is one of the most common tests, widely accessible, and it may provide at least two sets of experimental data: $\sigma_x(\varepsilon_x)$ and $\varepsilon_y(\varepsilon_x)$. The specific form of the scalar functions ϕ_1 and ϕ_2 for the case of a uniaxial stress state can be derived in the following way. Assuming that the direction of loading coincides with the x -direction ($\sigma_x \neq 0; \varepsilon_y^p = \varepsilon_z^p$), the scalar functions ϕ_1 and ϕ_2 become

$$\phi_1 = \frac{\varepsilon_x^p + 2\varepsilon_y^p}{\sigma_x}, \quad \phi_2 = \frac{|\varepsilon_x^p - \varepsilon_y^p|}{\sigma_x}. \quad (35)$$

Let us assume in the following an elastic-plastic material with linear hardening as shown in Fig. 2. The flow stress σ_x can be expressed in terms of the plastic modulus E^p as (cf. Fig. 2b)

$$\sigma_x(\varepsilon_x^p) = E^p \varepsilon_x^p + \sigma_s, \quad (36)$$

whereas the transversal deformation can be expressed as (cf. Fig. 2d)

$$\varepsilon_y(\varepsilon_x^p) = -\nu^p \varepsilon_x^p - \frac{\nu}{E} \sigma_s. \quad (37)$$

The plastic part of ε_y can be derived as

$$\varepsilon_y^p = \varepsilon_y - \varepsilon_y^e = -\nu^p \varepsilon_x^p - \frac{\nu}{E} \sigma_s + \nu \frac{\sigma_x}{E} = - \left(\nu^p - \nu \frac{E^p}{E} \right) \varepsilon_x^p, \quad (38)$$

¹ The last formula can be also justified by the fact that the tensors e^e , e^p and e are proportional to each other:

$$e^p = 2\mu\phi_2 e^e = \frac{1}{1+2\mu\phi_2} e.$$

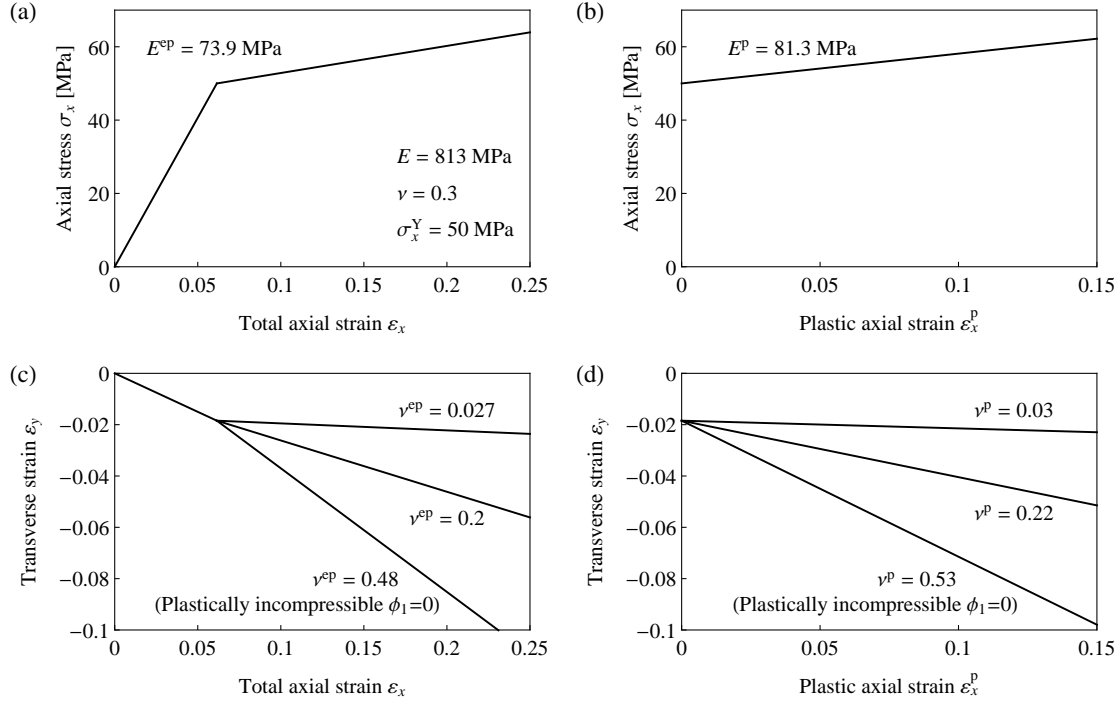


Figure 2: Example of constitutive behaviour in a uniaxial stress test for a linear hardening material: (a) Axial stress σ_x as a function of the total axial strain ϵ_x ; (b) Axial stress σ_x as a function of the plastic axial strain ϵ_x^p ; (c) Transverse contraction ϵ_y as a function of the total axial strain ϵ_x ; (d) Transverse contraction ϵ_y as a function of the plastic axial strain ϵ_x^p . Three cases of transverse contraction are considered: plastically incompressible material $\epsilon_m^p = 0$ ($\nu^{ep} = 0.48$ and $\nu^p = 0.53$), null plastic transverse contraction $\epsilon_y^p = 0$ ($\nu^{ep} = 0.027$ and $\nu^p = 0.03$) and an intermediate case ($\nu^{ep} = 0.2$ and $\nu^p = 0.22$).

so that the functions ϕ_1 and ϕ_2 are obtained in terms of the plastic strain in a uniaxial stress state as

$$\phi_1(\epsilon_x^p) = \frac{(E - 2\nu^p E + 2\nu E^p)\epsilon_x^p}{E(E^p \epsilon_x^p + \sigma_s)}, \quad \phi_2(\epsilon_x^p) = \frac{(E + \nu^p E - \nu E^p)\epsilon_x^p}{E(E^p \epsilon_x^p + \sigma_s)}. \quad (39)$$

Using the additive composition of the elastic and plastic strains, i. e. $\epsilon_x = \epsilon_x^e + \epsilon_x^p$, the stress σ_x and the transversal deformation ϵ_x^p are obtained as functions of the total strain ϵ_x

$$\sigma_x(\epsilon_x) = E^{ep} \epsilon_x + \frac{E - E^{ep}}{E} \sigma_s, \quad \epsilon_y(\epsilon_x) = -\nu^{ep} \epsilon_x - \frac{\nu - \nu^{ep}}{E} \sigma_s, \quad (40)$$

where

$$E^{ep} = \frac{E E^p}{E + E^p}, \quad \nu^{ep} = \frac{\nu^p E}{E + E^p}. \quad (41)$$

Finally, the dependence of ϕ_1 and ϕ_2 upon the total strain ε_x is given by

$$\phi_1(\varepsilon_x) = \frac{1}{E} \left(1 - 2\nu^p + 2\nu \frac{E^p}{E} \right) \frac{E\varepsilon_x - \sigma_s}{E^p\varepsilon_x + \sigma_s}, \quad (42)$$

$$\phi_2(\varepsilon_x) = \frac{1}{E} \left(1 + \nu^p - \nu \frac{E^p}{E} \right) \frac{E\varepsilon_x - \sigma_s}{E^p\varepsilon_x + \sigma_s}. \quad (43)$$

The functions $\phi_1(\varepsilon_x)$ and $\phi_2(\varepsilon_x)$ corresponding to the material parameters presented in Fig. 2 are shown in Fig. 3. Interestingly, in the case of uniaxial stress state the ratio of the functions $\phi_1(\varepsilon_x)$

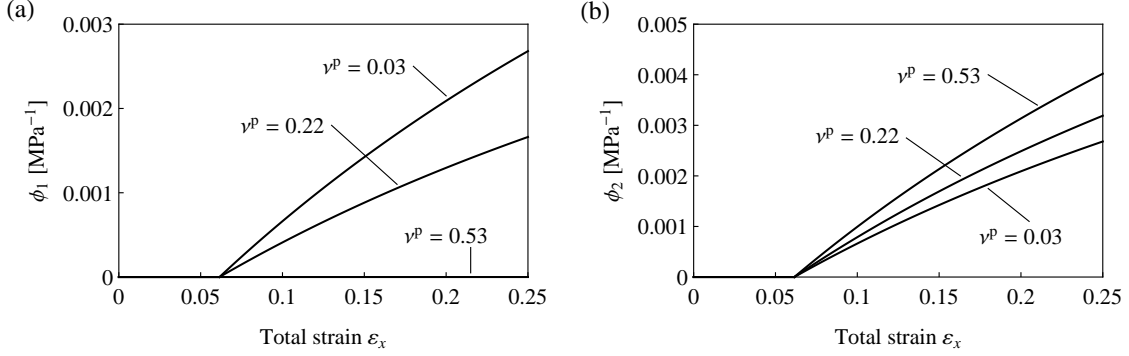


Figure 3: (a) Function $\phi_1(\varepsilon_x)$ and (b) function $\phi_2(\varepsilon_x)$ corresponding to the material parameters presented in Fig. 2.

and $\phi_2(\varepsilon_x)$ is a constant value:

$$\frac{\phi_1(\varepsilon_x)}{\phi_2(\varepsilon_x)} = \frac{(1 - 2\nu^p)E + 2\nu E^p}{(1 + \nu^p)E - \nu E^p}. \quad (44)$$

3.3 Pressure-dependent yielding: Drucker-Prager Material

Consider a material obeying the Drucker-Prager yield criterion,

$$F(J_1^\sigma, J_2^s) = \alpha J_1^\sigma + \sqrt{J_2^s} - k_s, \quad (45)$$

where $\alpha > 0$ is called pressure-sensitivity index and assumed to be a constant while k_s is a positive function of the plastic strain

$$k_s = k_s(\varepsilon^p) > 0. \quad (46)$$

In the case of uniaxial stress test

$$k_s(\varepsilon_x^p) = \alpha J_1^\sigma + \sqrt{J_2^s} = \left(\alpha + \frac{1}{\sqrt{3}} \right) (E^p \varepsilon_x^p + \sigma_s). \quad (47)$$

Assuming the normality rule (plastic strain increment proportional to the normal of the yield surface $n_{ij} = 2\alpha\sqrt{J_2^s}\delta_{ij} + s_{ij}$) and proportional loading we have (cf. [18])

$$\varepsilon_{ij}^p = \phi_2(2\alpha\sqrt{J_2^s}\delta_{ij} + s_{ij}), \quad (48)$$

so that

$$J_1^{\varepsilon^p} = 6\alpha\phi_2\sqrt{J_2^s}, \quad \sqrt{J_2^{e^p}} = \phi_2\sqrt{J_2^s}. \quad (49)$$

Note that the ratio between the two plastic strain invariants is constant

$$\frac{J_1^{\varepsilon^p}}{\sqrt{J_2^{e^p}}} = 6\alpha. \quad (50)$$

The general setting presented in Section 3.1 can be specialized to this type of material by defining

$$\phi_1 = \frac{6\alpha\sqrt{J_2^s}\phi_2}{J_1^\sigma}, \quad \phi_2 = \phi_2. \quad (51)$$

It is important to emphasize here that both functions ϕ_1 and ϕ_2 equal to zero simultaneously in the elastic regime or are both different from zero in the plastic zone.

We need to represent now the functions ϕ_1 and ϕ_2 depending only on the invariants of the total strain tensor. Let us assume that we have been successful with the second function,

$$\phi_2 = \phi_2(J_1^\varepsilon, J_2^e), \quad (52)$$

then the remaining function ϕ_1 can be computed from Eq. (51) under taking into account Eqs. (32), (25) and (26)

$$\phi_1 = 6\alpha\frac{\sqrt{J_2^s}\phi_2}{J_1^\sigma} = 6\alpha\phi_2\frac{2\tilde{\mu}}{3\tilde{K}}\frac{\sqrt{J_2^e}}{J_1^\varepsilon} = 6\alpha\phi_2\frac{1-2\nu+\phi_1E}{1+\nu+\phi_2E}\frac{\sqrt{J_2^e}}{J_1^\varepsilon}, \quad (53)$$

or

$$\phi_1 = \phi_1(J_1^\varepsilon, J_2^e) = \frac{6\alpha(1-2\nu)\phi_2\sqrt{J_2^e}}{J_1^\varepsilon(1+\nu)+\phi_2E(J_1^\varepsilon-6\alpha\sqrt{J_2^e})}. \quad (54)$$

Using Eqs. (52) and (54), the generalized elastic constants defined in Eqs. (25) and (26) can be rewritten in terms of the only two invariants of the total strain tensor:

$$\tilde{\mu}(\phi_2) = \tilde{G}(\phi_2) = \frac{E}{2(1+\nu+\phi_2E)}, \quad (55)$$

$$\tilde{E}(\phi_2) = \frac{3E}{1+\nu+\phi_2E}\frac{J_1^\varepsilon(1+\nu+\phi_2E)-6\alpha\phi_2E\sqrt{J_2^e}}{J_1^\varepsilon(3+2\phi_2E)-12\alpha\phi_2E\sqrt{J_2^e}}, \quad (56)$$

$$\tilde{\nu}(\phi_2) = \frac{J_1^\varepsilon(3\nu+\phi_2E)-6\alpha\phi_2E\sqrt{J_2^e}}{J_1^\varepsilon(3+2\phi_2E)-12\alpha\phi_2E\sqrt{J_2^e}}, \quad (57)$$

$$\tilde{K}(\phi_2) = \frac{J_1^\varepsilon(1+\nu+\phi_2E)-6\alpha\phi_2E\sqrt{J_2^e}}{3J_1^\varepsilon(1-2\nu)(1+\nu+\phi_2E)}E. \quad (58)$$

Finally, the multiaxial hardening law for a linear hardening material (cf. Fig. 2) can be obtained from the uniaxial one, Eq. (47), by substituting ε_x^p with the equivalent plastic strain, which can be defined for the Drucker-Prager material as

$$\varepsilon^p = \frac{\sqrt{3}E}{(1+\nu^p)E-\nu E^p}\sqrt{J_2^{e^p}} = \frac{2(\sqrt{3}+3\alpha)}{3}\sqrt{J_2^{e^p}}. \quad (59)$$

This gives

$$k_s \left(\sqrt{J_2^{ep}} \right) = \alpha J_1^\sigma + \sqrt{J_2^s} = \left(\alpha + \frac{1}{\sqrt{3}} \right) \left(\omega \sqrt{J_2^{ep}} + \sigma_s \right), \quad (60)$$

where

$$\omega = \frac{\sqrt{3}E^p E}{(1 + \nu^p)E - \nu E^p} = \frac{2E^p(\sqrt{3} + 3\alpha)}{3}. \quad (61)$$

In case of the uniaxial stress test discussed in the previous section, Eqs. (44) and (51) allow us to determine the unknown parameter $\alpha > 0$ from the experiment

$$\alpha = \frac{J_1^\sigma (1 - 2\nu^p)E + 2\nu E^p}{6\sqrt{J_2^s} (1 + \nu^p)E - \nu E^p} = \frac{1}{2\sqrt{3}} \frac{(1 - 2\nu^p)E + 2\nu E^p}{(1 + \nu^p)E - \nu E^p} < \frac{1}{2\sqrt{3}}. \quad (62)$$

Thus, to complete the analysis, the only unknown function ϕ_2 should be defined. In general, this function depends on both strain invariants J_1^ε and J_2^e

$$\phi_2 = \phi_2(J_1^\varepsilon, J_2^e). \quad (63)$$

To this end, note that we can eliminate J_1^σ and J_1^{ep} from Eqs. (34)₁, (50) and then solve Eqs. (34)₁, (60) to obtain $J_2^s(J_1^\varepsilon, J_2^e)$ and $J_2^{ep}(J_1^\varepsilon, J_2^e)$. The function $\phi_2(J_1^\varepsilon, J_2^e)$ is then derived as

$$\phi_2(J_1^\varepsilon, J_2^e) = \frac{\sqrt{J_2^s}}{\sqrt{J_2^{ep}}} = \frac{3\alpha(1 + \nu)EJ_1^\varepsilon + (1 - 2\nu) [3E\sqrt{J_2^e} - (3\alpha + \sqrt{3})(1 + \nu)\sigma_s]}{E \{ 18\alpha^2 E \sqrt{J_2^e} - 3\alpha [EJ_1^\varepsilon - (1 - 2\nu)(\omega\sqrt{J_2^e} + \sigma_s)] + \sqrt{3}(1 - 2\nu)(\omega\sqrt{J_2^e} + \sigma_s) \}}. \quad (64)$$

Finally, the function $\phi_1(J_1^\varepsilon, J_2^e)$ is obtained from (54)

$$\phi_1(J_1^\varepsilon, J_2^e) = \frac{6\alpha \{ 3\alpha(1 + \nu)EJ_1^\varepsilon + (1 - 2\nu) [3E\sqrt{J_2^e} - (3\alpha + \sqrt{3})(1 + \nu)\sigma_s] \}}{E [3E(J_1^\varepsilon - 6\alpha\sqrt{J_2^e}) + (3\alpha + \sqrt{3})(1 + \nu)(\omega J_1^\varepsilon + 6\alpha\sigma_s)]}. \quad (65)$$

The evaluation of the functions ϕ_1 and ϕ_2 of the two strain invariants J_1^ε and J_2^e for a Drucker-Prager material having the uniaxial stress-strain curve given in Fig. 2 ($E = 813$ MPa; $\nu = 0.3$; $\sigma_s = 50$ MPa; $E^p = 81.3$ MPa; $\nu^{ep} = 0.2$; $\nu^p = 0.22$) is shown in Fig. 4. It is noted that the function ϕ_1 shows a discontinuity line emanating from a pure shear state on the yield surface and separating regions of different sign. The function ϕ_2 also shows a discontinuity line emanating from the vertex of the Drucker-Prager cone.

The deformation theory developed in this section for Drucker-Prager material with linear hardening has been validated by comparison with the flow theory for several monotonic loadings. Finite element simulations on a single element with displacement control have been performed in ABAQUS and results (not reported here) are always in agreement with the deformation theory.

We present here two examples of monotonic loadings, designed in such a way to investigate the discontinuities shown by the functions ϕ_1 and ϕ_2 . It will be seen that these discontinuities are genuine features of the Drucker-Prager model with associated flow rule and are obtained also by the more rigorous flow theory of plasticity.

In the first example, the following monotonic loading has been applied in two steps (see Fig. 5): first a dilatational deformation (from point O to point A in Fig. 5a), followed by an isochoric

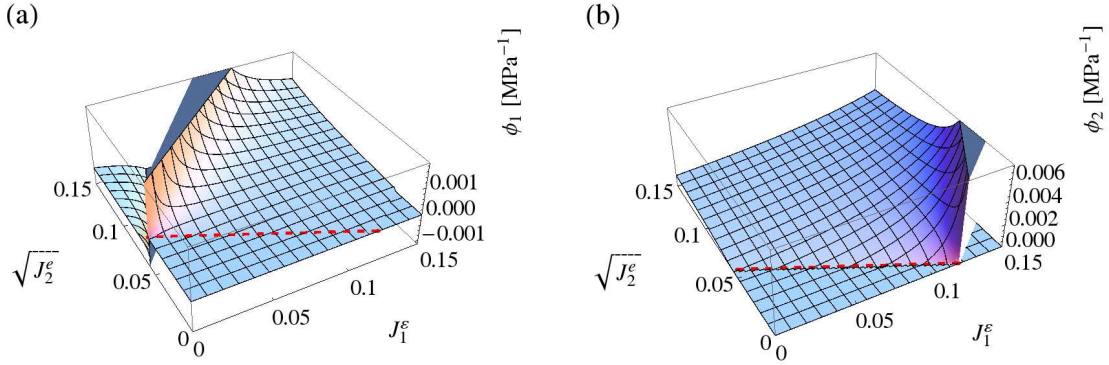


Figure 4: (a) Function ϕ_1 and (b) function ϕ_2 of Drucker-Prager's material with linear hardening as functions of the two invariants of strain, J_1^e and J_2^e . The dashed red line indicates the elastic limit.

deformation (shearing in the plane x_1 - x_2 , from point A to point B in Fig. 5a). This specific loading path has been chosen as it crosses the discontinuity line for the function ϕ_1 . The value of the function ϕ_1 along the isochoric path AB is shown in Fig. 5b: results of finite element simulation and deformation theory are in agreement.

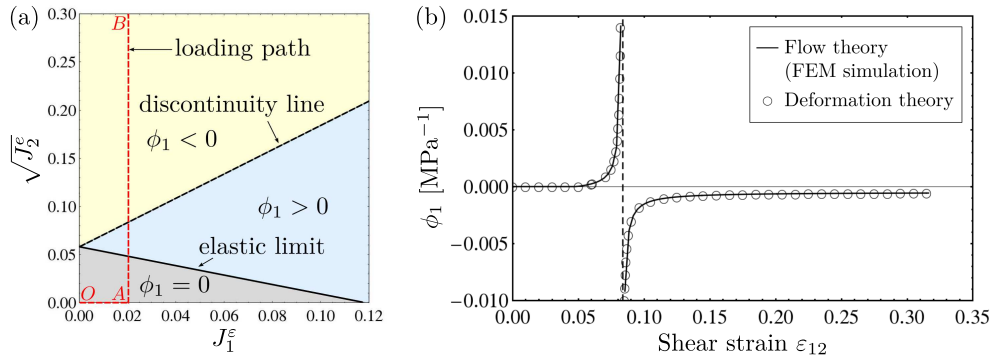


Figure 5: (a) Function ϕ_1 in the J_1^e - $\sqrt{J_2^e}$ plane: elastic domain $\phi_1 = 0$ (light grey), plastic domain with a discontinuity line separating the regions $\phi_1 > 0$ (light blue) and $\phi_1 < 0$ (light yellow). The red dashed line indicates the loading path. (b) Function ϕ_1 along the isochoric path AB . The discontinuity is clearly visible and results of finite element simulation and deformation theory are in agreement.

In Fig. 6, we present the stress-strain curves along the isochoric path AB of Fig. 5a. In particular, Fig. 6a shows the shear stress σ_{12} and Fig. 6b the normal stress σ_{11} , both as a function of the shear strain ϵ_{12} . The agreement between flow theory (finite element simulation) and deformation theory is excellent. It is noted also that the singularity of the function ϕ_1 does not invalidate the results of the deformation theory model, as the deformation can be continued beyond the discontinuity line.

In the second example, the following monotonic loading has been applied in two steps (see

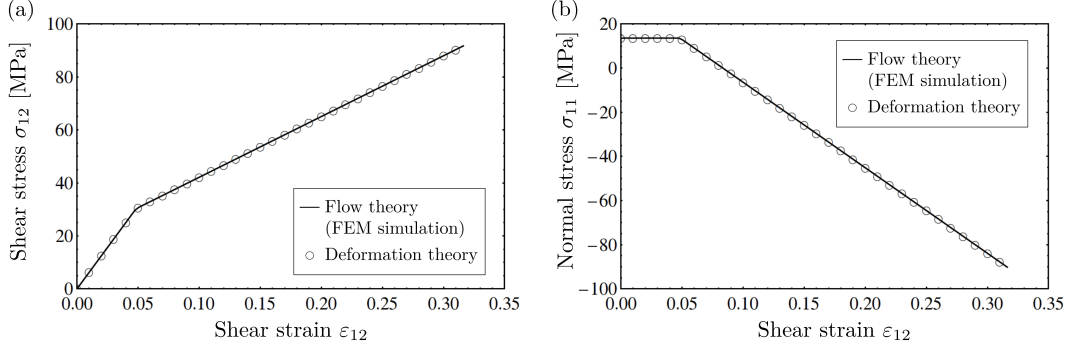


Figure 6: Response of the material in terms of stress-strain curves along the isochoric path AB of Fig. 5a: (a) shear stress σ_{12} ; (b) normal stress σ_{11} .

Fig. 7): first a isochoric deformation (shearing in the plane x_1 - x_2 , from point O to point A in Fig. 7a), followed by a dilatational deformation (from point A to point B in Fig. 7a). This specific loading path has been chosen as it crosses the discontinuity line for the function ϕ_2 . The value of the function ϕ_2 along the dilatational path AB is shown in Fig. 7b: results of finite element simulation and deformation theory are in agreement.

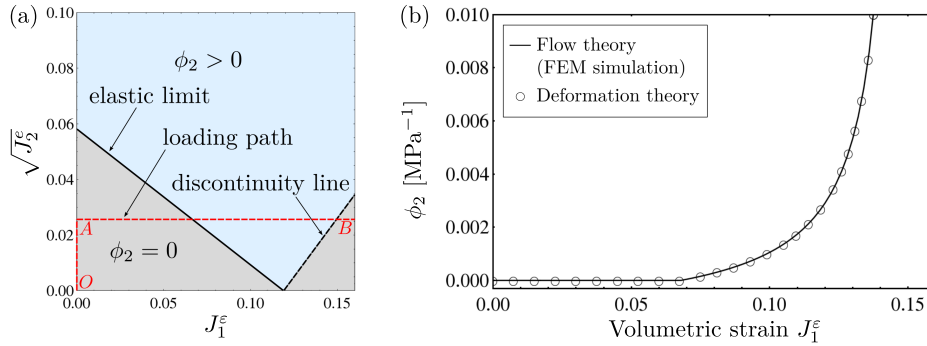


Figure 7: (a) Function ϕ_2 in the J_1^e - $\sqrt{J_2^e}$ plane: elastic domain $\phi_2 = 0$ (light grey), plastic domain with a discontinuity line separating the regions $\phi_2 > 0$ (light blue) and $\phi_2 = 0$ (light grey). The red dashed line indicates the loading path. (b) Function ϕ_2 along the dilatational path AB . The discontinuity is clearly visible and results of finite element simulation and deformation theory are in agreement.

In Fig. 8, we present the stress-strain curves along the dilatational path AB of Fig. 7a. In particular, Fig. 8a shows the shear stress σ_{12} and Fig. 8b the normal stress σ_{11} , both as a function of the dilatational strain ϵ_{11} . Again, the agreement between flow theory (finite element simulation) and deformation theory is excellent. However, now the deformation cannot be continued beyond the discontinuity line, as the function ϕ_2 would become negative, which is unphysical. This is due to the fact that the Drucker-Prager model with associate plastic flow always predicts plastic dilatancy.

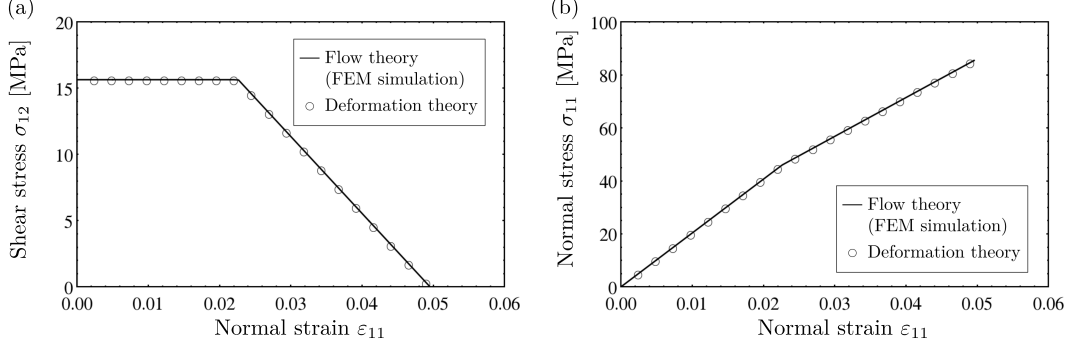


Figure 8: Response of the material in terms of stress-strain curves along the dilatational path AB of Fig. 7a: (a) shear stress σ_{12} ; (b) normal stress σ_{11} .

3.4 Plane strain formulation of transmission conditions

The two-dimensional plane strain formulation is relevant for the analysis if the conditions of the plane strain are satisfied in the system, i.e. the following components of the strain and stress tensors vanish within the interphase:

$$\varepsilon_{j3} = 0, \quad \sigma_{i3} = 0, \quad j = 1, 2, 3, \quad i = 1, 2, \quad (66)$$

while the remaining components are functions of the independent variables x_1 and x_2 only.

Finally, the remaining component of the stress tensor can be evaluated from

$$\sigma_{33} = (\varepsilon_{11} + \varepsilon_{22})\tilde{\lambda}(\phi_1, \phi_2). \quad (67)$$

Taking into account (66) and the Hooke's law (1), we obtain the leading terms of the strain tensor invariants [16]:

$$J_1^\varepsilon = \frac{\partial u_2}{\partial x_2} = \frac{\sigma_{22}}{\tilde{\lambda} + 2\tilde{\mu}}, \quad (68)$$

$$J_2^\varepsilon = \frac{1}{3} \left(\frac{\partial u_2}{\partial x_2} \right)^2 + \frac{1}{4} \left(\frac{\partial u_1}{\partial x_2} \right)^2 = \frac{1}{3} \frac{\sigma_{22}^2}{(\tilde{\lambda} + 2\tilde{\mu})^2} + \frac{1}{4} \frac{\sigma_{12}^2}{\tilde{\mu}^2}. \quad (69)$$

Moreover, all the strain and stress components here are functions only of the spatial variable x_1 . Finally, relationship (16) remains valid, while (17) is rewritten in the form:

$$J_2^e = \frac{1}{12h^2} \llbracket u_2 \rrbracket^2 + \frac{1}{16h^2} \llbracket u_1 \rrbracket^2. \quad (70)$$

Note that the transmission conditions (7) and (8) are defined now for the two-components vectors $\mathbf{t}_2 = [\sigma_{21}, \sigma_{22}]^T$, $\mathbf{u} = [u_1, u_2]^T$ and the matrix \mathbf{A} is given by

$$\mathbf{A} = \begin{pmatrix} \tilde{\mu} & 0 \\ 0 & \tilde{\lambda} + 2\tilde{\mu} \end{pmatrix}. \quad (71)$$

It should be noted that the transmission conditions for plane strain conditions can be written in the compact form as

$$\llbracket \sigma_{12} \rrbracket = 0, \quad \llbracket \sigma_{22} \rrbracket = 0, \quad \sigma_{12} = F_1(\llbracket u_1 \rrbracket, \llbracket u_2 \rrbracket), \quad \sigma_{22} = F_2(\llbracket u_1 \rrbracket, \llbracket u_2 \rrbracket), \quad (72)$$

where the functions F_1 and F_2 are given by

$$F_1 = \frac{1}{2h} \tilde{\mu}(\phi_1, \phi_2) \llbracket u_1 \rrbracket, \quad F_2 = \frac{1}{2h} (\tilde{\lambda} + 2\tilde{\mu})(\phi_1, \phi_2) \llbracket u_2 \rrbracket. \quad (73)$$

4 Validation of the nonlinear transmission conditions for elastoplastic pressure-dependent interphases

The geometry of the considered structure is shown in Fig. 9. In the analysis the two bonded materials are assumed to be identical and linear elastic, with Young's modulus $E_{\pm} = 72700$ MPa and Poisson's ratio $\nu_{\pm} = 0.34$. The geometrical dimensions are $L = 10$ mm, $H = 1$ mm, and $2h = 0.01$ mm. As a result, the small parameter takes the value $\epsilon = 2h/H = 0.01$, which is small enough to justify our asymptotic model.

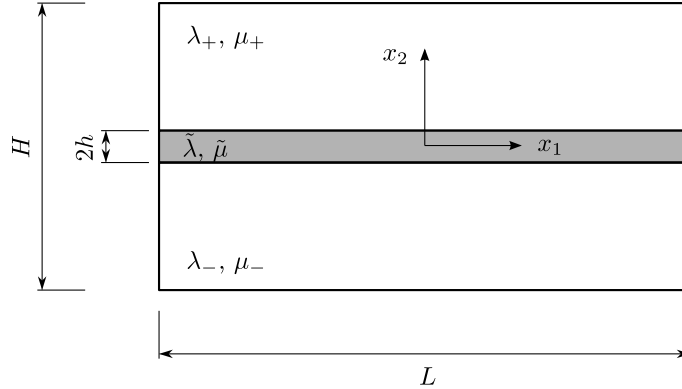


Figure 9: Geometry of the three-phase structure.

A linear elastic-linear hardening Drucker-Prager model (pressure-dependent yielding) is assumed for the adhesive material within the interphase. The material parameters are defined in Tab. 1 and the corresponding stress-strain curve in uniaxial stress test is shown in Fig. 3a. For comparison with known results in the literature, a linear elastic-linear hardening von Mises model (pressure-independent yielding) is also considered. All the analyses performed with the von Mises model are in agreement with the literature and are not shown here.

The commercial finite element code ABAQUS is used for the simulation of the mechanical behaviour of the three-phase structure and validation of transmission conditions (72). The transmission conditions are based on the deformation theory of plasticity developed in Section 3, whereas the FEM simulations are based on the more general theory of plastic flow. For this reason, only monotonic external loading is considered in the simulations.

The two-dimensional FE-mesh is shown in Fig. 10. It has been generated automatically using the mesh generator available within ABAQUS with 4-node bilinear, reduced integration elements with

| Material | E (MPa) | ν | σ_s (MPa) | E^p (MPa) | ν^p | α |
|----------------|--------------|-------|---------------------|----------------|---------|----------|
| Drucker-Prager | 813 | 0.3 | 50 | 81.3 | 0.22 | 0.1504 |
| von Mises | 813 | 0.3 | 50 | 81.3 | 0.53 | 0 |

Table 1: Material parameters used for the validation of transmission conditions.

hourglass control (CPE4R). A strong mesh refinement is used within the intermediate elastoplastic layer. The mesh consists of 757774 nodes and 757599 elements.

The validation of transmission conditions is performed as follows. From the FEM simulation we obtain the displacements at the top ($x_2 = h$) and bottom ($x_2 = -h$) of the intermediate layer and evaluate the jumps $\llbracket u_1 \rrbracket$ and $\llbracket u_2 \rrbracket$. Then, we can compute in sequence: the strain invariants J_1^ε and J_2^ε from (16) and (70), the functions ϕ_1 and ϕ_2 involved in the deformation theory from (65) and (64), the generalized Lamé constants λ and $\tilde{\mu}$ from (25), and finally the tractions predicted by the transmission conditions $F_1(\llbracket u_1 \rrbracket, \llbracket u_2 \rrbracket)$ and $F_2(\llbracket u_1 \rrbracket, \llbracket u_2 \rrbracket)$ from (73). The final check consists in comparing the predicted tractions with those obtained from the FEM simulation.

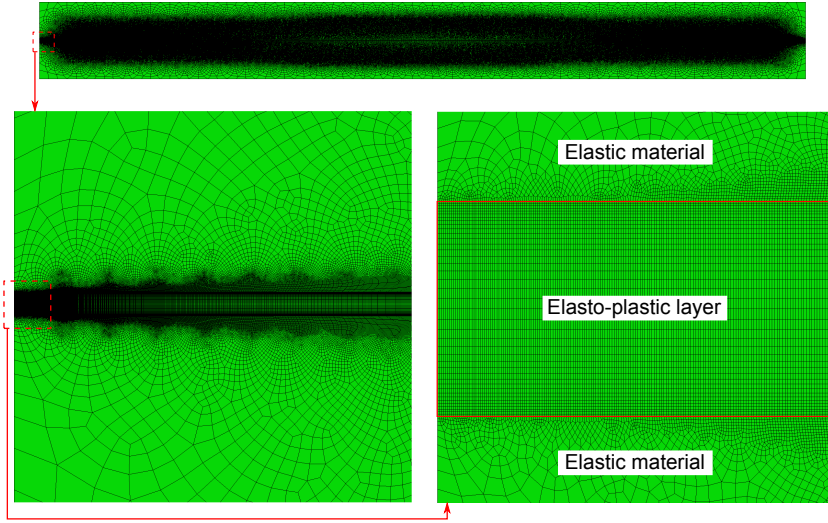


Figure 10: Two-dimensional FE-mesh.

4.1 Tensile loading with fixed grips

A monotonic tensile loading with fixed grips ($u_1(x_1, H/2) = 0$, $u_2(x_1, H/2) = v_2$) is applied to the top of the bimaterial structure in the range of v_2/H from 0% to 0.3% in 100 fixed increments, see Fig. 11.

The equivalent stress and the equivalent plastic strain along a horizontal line in the middle of

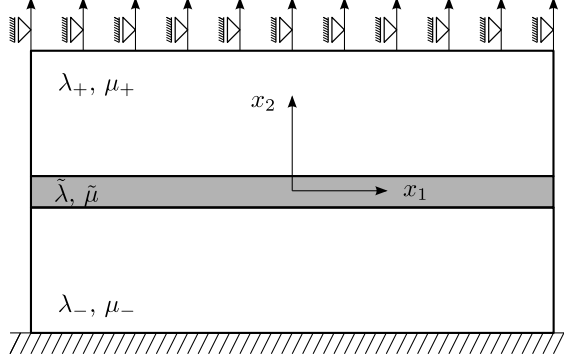


Figure 11: Tensile loading with fixed grips.

the interphase are shown in Fig. 12, every ten increments. It is noted that at the 10th ($v_2/H = 0.03\%$), 20th ($v_2/H = 0.06\%$) and 30th ($v_2/H = 0.09\%$) increments the interphase is still in the elastic regime. A visible plastic zone appears in the middle of the interphase at the 40th increment ($v_2/H = 0.12\%$). At the 50th increment ($v_2/H = 0.15\%$), the interphase is fully plasticised.

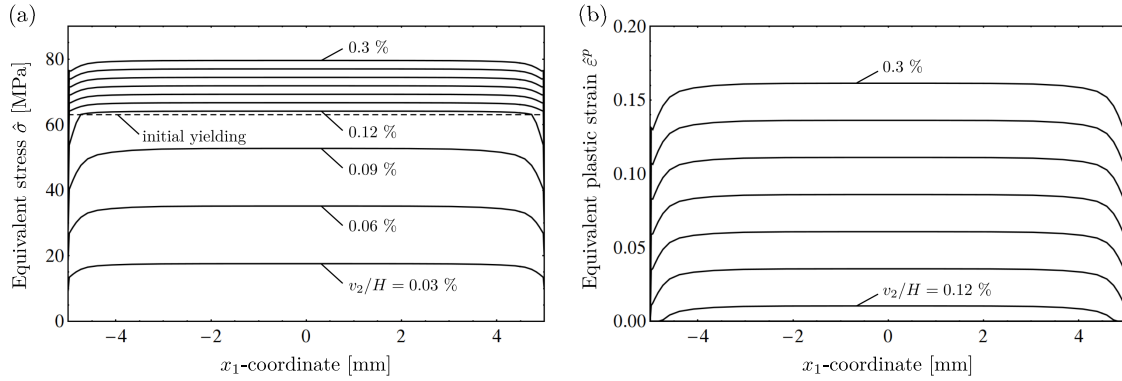


Figure 12: Distribution of equivalent stress (a) and equivalent plastic strain (b) along the interphase for different levels of deformation (tensile loading with fixed grips).

Due to the symmetry of the considered problem (geometry and applied loading), three of the transmission conditions, i.e. $[[\sigma_{12}]] = [[\sigma_{22}]] = 0$ and $F_1([[u_1]], [[u_2]]) = \sigma_{12}$, are identically satisfied, because $[[u_1]] = 0$ and $\sigma_{12} = 0$ hold in this case. The remaining condition $F_2(0, [[u_2]]) = \sigma_{22}$ has to be verified.

In Fig. 13(a), comparisons of the left and right hand sides of the condition $F_2(0, [[u_2]]) = \sigma_{22}$ are presented. The accuracy of the transmission condition is excellent, both in the elastic and plastic regimes, along the whole interface except for a very small edge zone, as shown in Fig. 13(b), where a magnification of the same functions in the interval $4.95 < x_1 < 5$ at the right boundary is presented. The size of this edge region is typically 3–4 times the thickness of the interphase.

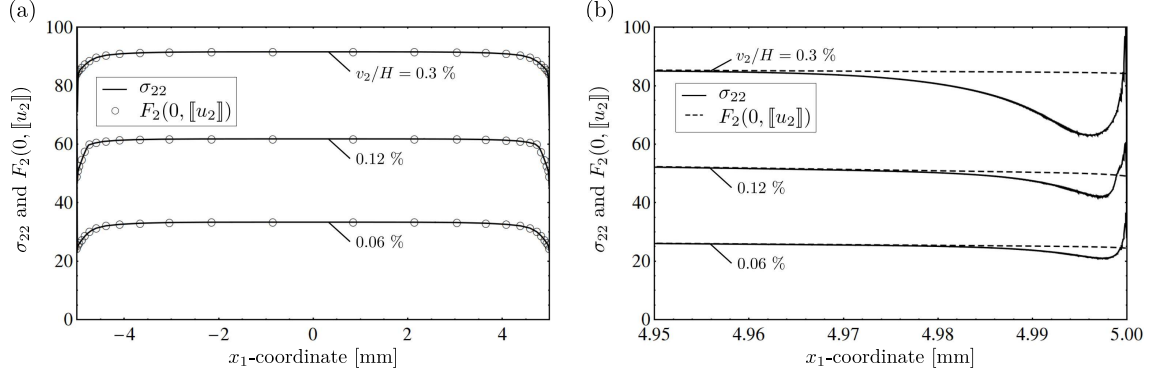


Figure 13: (a) Validation of the transmission condition $F_2(0, \llbracket u_2 \rrbracket) = \sigma_{22}$ for a pressure-sensitivity elastoplastic interphase (tensile loading with fixed grips). (b) Magnification of the same functions in the interval $4.95 < x_1 < 5$ at the right boundary.

4.2 Shear loading

A monotonic shear loading ($u_1(x_1, H/2) = v_1$, $u_2(x_1, H/2) = 0$) is applied to the top of the bi-material structure in the range of v_1/H from 0% to 0.7% in 100 fixed increments, see Fig. 14.

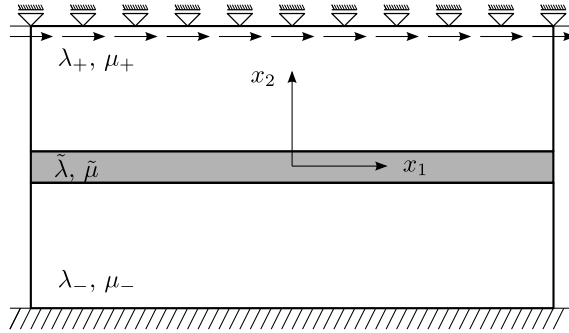


Figure 14: Shear loading.

The equivalent stress and the equivalent plastic strain along a horizontal line in the middle of the interphase are shown in Fig. 15, every ten increments. It is noted that at the 10th ($v_1/H = 0.07\%$), 20th ($v_1/H = 0.14\%$), and 30th ($v_1/H = 0.21\%$) increments the interphase is still in the elastic regime. A visible plastic zone appears in the middle of the interphase at the 40th increment ($v_1/H = 0.28\%$). At the 50th increment ($v_1/H = 0.35\%$), the interphase is fully plasticised.

Due to the anti-symmetry of the considered problem (geometry and applied loading), two of the transmission conditions, i.e. $\llbracket \sigma_{12} \rrbracket = \llbracket \sigma_{22} \rrbracket = 0$, are identically satisfied. The remaining conditions $F_1(\llbracket u_1 \rrbracket, \llbracket u_2 \rrbracket) = \sigma_{12}$ and $F_2(\llbracket u_1 \rrbracket, \llbracket u_2 \rrbracket) = \sigma_{22}$ have to be verified. In fact, due to the dilatancy of plastic deformation typical of the Drucker-Prager model, we have $\llbracket u_2 \rrbracket \neq 0$ and, consequently, tensile stress develops within the interphase, $\sigma_{22} \neq 0$.

In Fig. 16(a), comparisons of the left and right hand sides of the condition $F_1(\llbracket u_1 \rrbracket, \llbracket u_2 \rrbracket) = \sigma_{12}$

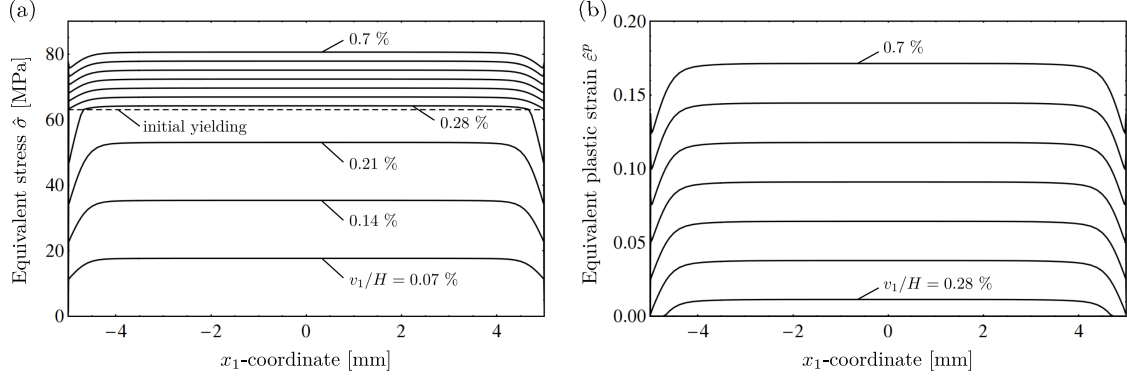


Figure 15: Distribution of equivalent stress (a) and equivalent plastic strain (b) along the interphase for different levels of deformation (shear loading).

are presented. The accuracy of the transmission condition is excellent, both in the elastic and plastic regimes, along the whole interface except for a very small edge zone, as shown in Fig. 16(b), where a magnification of the same functions in the interval $4.95 < x_1 < 5$ at the right boundary is presented. The size of this edge region is typically 3–4 times the thickness of the interphase.

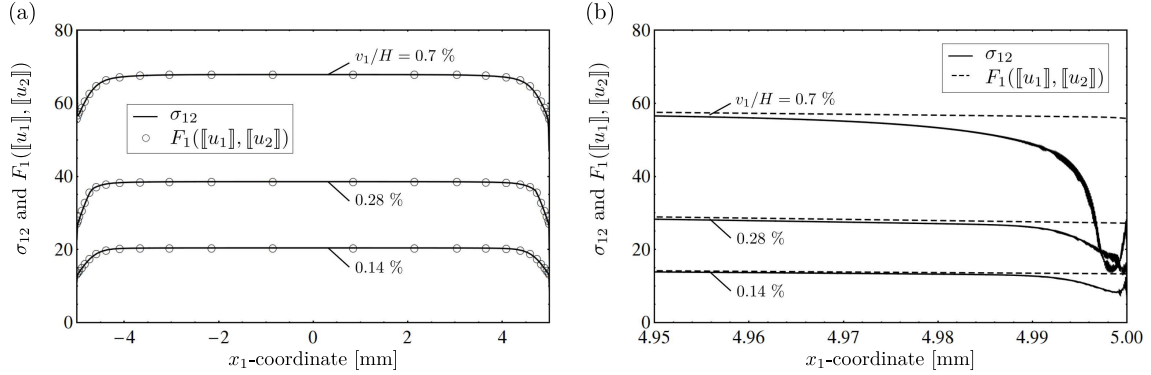


Figure 16: (a) Validation of the transmission condition $F_1(\llbracket u_1 \rrbracket, \llbracket u_2 \rrbracket) = \sigma_{12}$ for a pressure-sensitivity elastoplastic interphase (shear loading). (b) Magnification of the same functions in the interval $4.95 < x_1 < 5$ at the right boundary.

In Fig. 17(a), comparisons of the left and right hand sides of the condition $F_2(\llbracket u_1 \rrbracket, \llbracket u_2 \rrbracket) = \sigma_{22}$ are presented. In this case, the accuracy of the transmission condition is still excellent in the elastic regime ($v_1/H = 0.14\%$) and in the early stage of plastic deformation ($v_1/H = 0.28\%$). However, at later stages of plastic deformation ($v_1/H = 0.7\%$) the prediction of the transmission condition appears to be less accurate.

We observe that, the ellipticity conditions for the generalized elastic constants are not satisfied in the considered stages of plastic deformation ($v_1/H = 0.28\%$ and $v_1/H = 0.7\%$), see Fig. 18. In particular, the generalized bulk modulus \tilde{K} becomes negative and, consequently, the generalized Poisson's coefficient exceeds 0.5. This behaviour is intrinsic of the Drucker-Prager model with

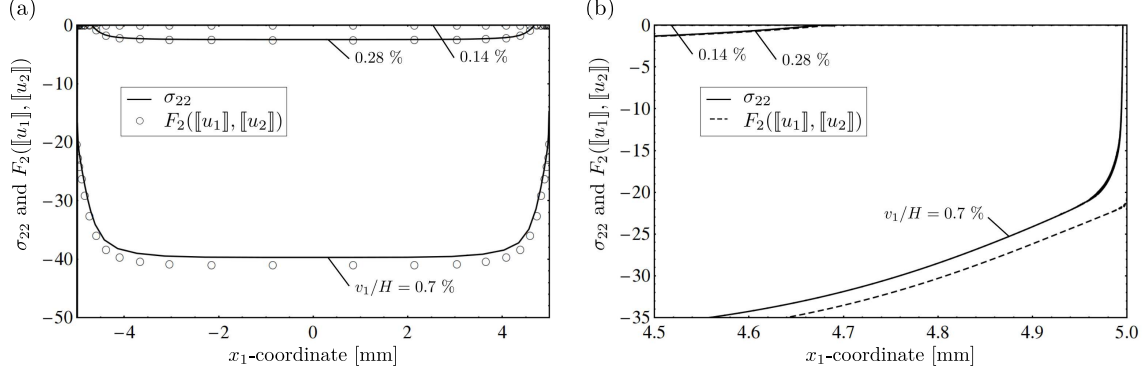


Figure 17: (a) Validation of the transmission condition $F_2([u_1], [u_2]) = \sigma_{22}$ for a pressure-sensitivity elastoplastic interphase (shear loading). (b) Magnification of the same functions in the interval $4.5 < x_1 < 5$ at the right boundary.

associated plastic flow, which always predicts plastic dilatancy.

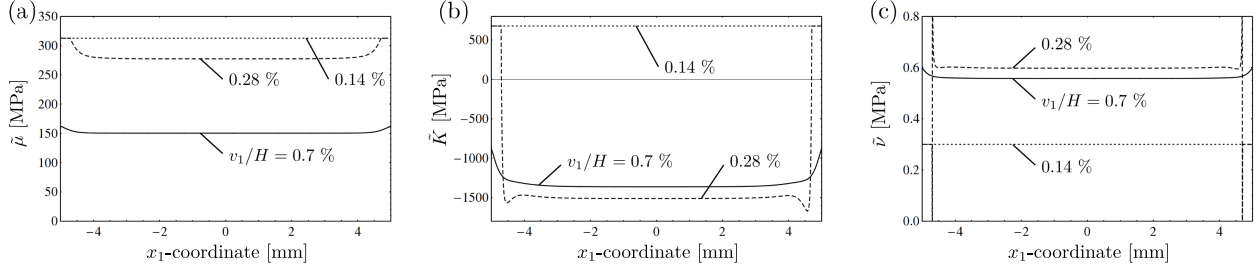


Figure 18: Generalized elastic constants $\tilde{\mu}$ (a), \tilde{K} (b), $\tilde{\nu}$ (c), for different levels of deformation (shear loading).

4.3 Combined loading

A combined loading is applied to the top of the specimen in such a way that the same displacements are prescribed in the x_1 as well as the x_2 directions ($u_1(x_1, H/2) = u_2(x_1, H/2) = v$) in the range of v/H from 0% to 0.35% in 100 fixed increments, see Fig. 19.

The equivalent stress and the equivalent plastic strain along a horizontal line in the middle of the interphase are shown in Fig. 20, every ten increments. It is noted that at the 10th ($v_1/H = 0.06\%$) and 20th ($v_1/H = 0.12\%$) increments the interphase is still in the elastic regime. A visible plastic zone appears in the middle of the interphase at the 30th increment ($v_1/H = 0.18\%$). At the 40th increment ($v_1/H = 0.24\%$), the interphase is fully plasticised.

For this type of loading, the two conditions $F_1([u_1], [u_2]) = \sigma_{12}$ and $F_2([u_1], [u_2]) = \sigma_{22}$ have to be verified. In Fig. 21(a), comparisons of the left and right hand sides of the condition $F_2([u_1], [u_2]) = \sigma_{22}$ are presented. The accuracy of the transmission condition is excellent for all stages of deformation. In Fig. 22(a), comparisons of the left and right hand sides of the condition $F_1([u_1], [u_2]) = \sigma_{12}$ are presented.

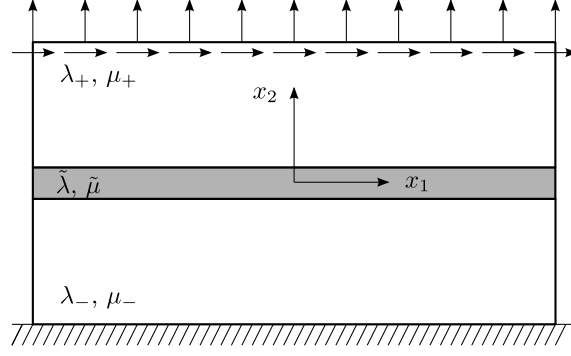


Figure 19: Combined loading.

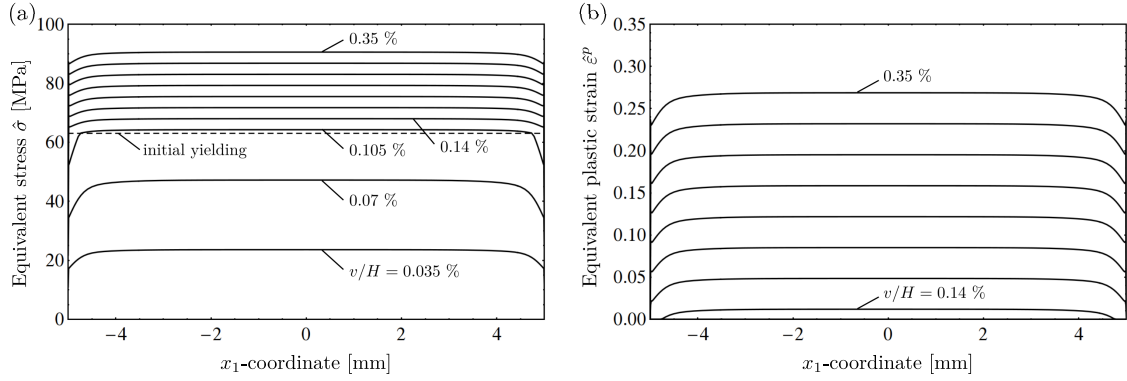


Figure 20: Distribution of equivalent stress (a) and equivalent plastic strain (b) along the interphase for different levels of deformation (combined loading).

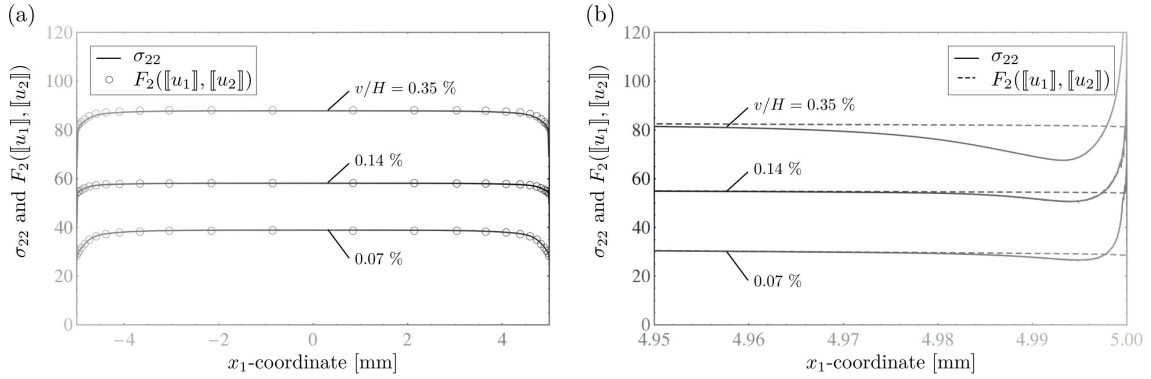


Figure 21: (a) Validation of the transmission condition $F_2(\llbracket u_1 \rrbracket, \llbracket u_2 \rrbracket) = \sigma_{22}$ for a pressure-sensitivity elastoplastic interphase (combined loading). (b) Magnification of the same functions in the interval $4.95 < x_1 < 5$ at the right boundary.

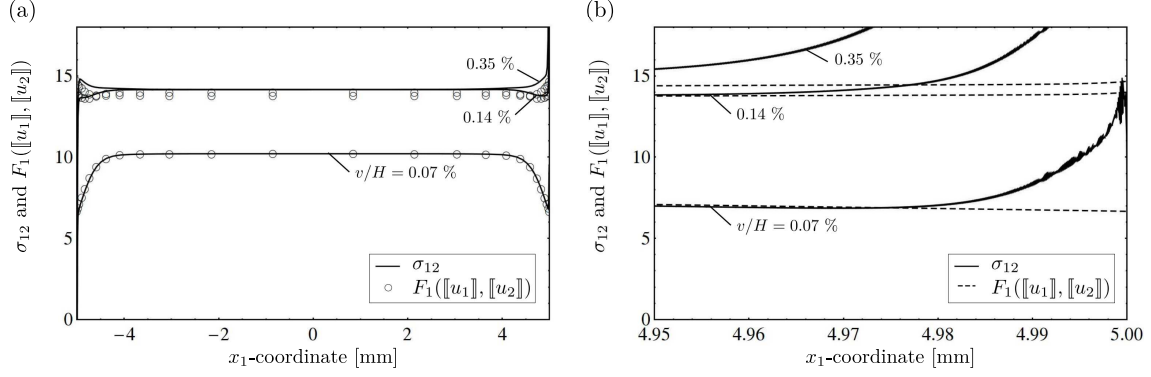


Figure 22: (a) Validation of the transmission condition $F_1(\llbracket u_1 \rrbracket, \llbracket u_2 \rrbracket) = \sigma_{12}$ for a pressure-sensitivity elastoplastic interphase (combined loading). (b) Magnification of the same functions in the interval $4.95 < x_1 < 5$ at the right boundary.

5 Conclusions

We have proven that a thin interphase consisting of a soft elasto-plastic pressure dependent material can be effectively modelled by an imperfect nonlinear interface. The latter is governed by nonlinear transmission conditions prescribed along the infinitesimal interface separating two different materials and incorporating the material properties of the adhesive material. The transmission conditions evaluated here differ essentially from those previously delivered for the case of von Mises plastic law [13, 14]. Indeed, the phenomenological functions ϕ_1 and ϕ_2 describing the equivalent elasto-plastic interface are not smooth and exhibit a singular behaviour having clear physical sense. Moreover, the conditions evaluated here are universal, in comparison with those delivered previously [16], and can be used for arbitrary stress-state of the considered three-phase body. This makes the evaluated transmission conditions widely applicable and ready to use in FEM analyses (for instance as traction-separation laws in cohesive element formulations) in order to model very thin adhesive layers. This approach avoids extreme mesh refinements usually needed in standard approaches.

The transmission conditions are validated by numerical examples based on accurate finite element simulations. The accuracy and efficiency of the proposed approach prove to be very high for different monotonic loading conditions. However, as it is the case of any imperfect interface, the conditions are valid along the whole interface apart from a small region close to the sample boundaries where the edge effect is playing a decisive role. To tackle this phenomenon, one needs additionally to use special FEM elements properly modelling the local stress-strain field. Such strategy (imperfect interface approach enriched by the edge special elements) is an efficient way to compute the details of a structure containing extremely thin soft elasto-plastic interphases of various plastic properties, at least in case of monotonic loading. In case of cyclic load, the range of applicability of the transmission conditions is still to be analysed.

Acknowledgements A.P. gratefully thanks financial support of the Italian Ministry of Education, University and Research in the framework of the FIRB project 2010 “Structural mechanics models

for renewable energy applications”, G.M. and W.M. gratefully acknowledges the support from the European Union Seventh Framework Programme under contract numbers PIAP-GA-2011-286110-INTERCER2 and PIAP-GA-2011-284544-PARM2, respectively.

References

- [1] B. Golaz, V. Michaud, S. Lavanchy, and J.-A.E. MÅñson. Design and durability of titanium adhesive joints for marine applications. *Int. J. Adhesion Adhesives*, 45:150–157, 2013.
- [2] S. Bhowmik, R. Benedictus, J.A. Poulis, H.W. Bonin, and V.T. Bui. High-performance nanoadhesive bonding of titanium for aerospace and space applications. *Int. J. Adhesion Adhesives*, 29(3):259–267, 2009.
- [3] A.L. Loureiro, L.F.M. Da Silva, C. Sato, and M.A.V. Figueiredo. Comparison of the mechanical behaviour between stiff and flexible adhesive joints for the automotive industry. *J. Adhesion*, 86(7):765–787, 2010.
- [4] J.J. Bikerman. *The science of adhesive joints*. Academic Press, New York, 1961.
- [5] R.D. Adams and N.A. Peppiatt. Stress analysis of adhesive-bonded lap joints. *J Strain Anal*, 9(3):185–196, 1974.
- [6] C.H. Wang and P. Chalkley. Plastic yielding of a film adhesive under multiaxial stresses. *Int. J. Adhesion Adhesives*, 20(2):155–164, 2000.
- [7] S. Rabinowitz, I.M. Ward, and J.S.C. Parry. The effect of hydrostatic pressure on the shear yield behaviour of polymers. *J. Mater. Sci.*, 5(1):29–39, 1970.
- [8] H. Altenbach and K. Tushtev. A new static failure criterion for isotropic polymers. *Mech. Compos. Mater.*, 37(5-6):475–482, 2001.
- [9] Y. Benveniste. The effective mechanical behaviour of composite materials with imperfect contact between the constituents. *Mech. Mater.*, 4(2):197–208, 1985.
- [10] Y. Benveniste and T. Miloh. Imperfect soft and stiff interfaces in two-dimensional elasticity. *Mech. Mater.*, 33(6):309–323, 2001.
- [11] O. Avila-Pozos, A. Klarbring, and A.B. Movchan. Asymptotic model of orthotropic highly inhomogeneous layered structure. *Mech. Mater.*, 31(2):101–115, 1999.
- [12] Z. Hashin. Thin interphase/imperfect interface in elasticity with application to coated fiber composites. *J. Mech. Phys. Solids*, 50(12):2509–2537, 2002.
- [13] T. Ikeda, A. Yamashita, D. Lee, and N. Miyazaki. Failure of a ductile adhesive layer constrained by hard adherends. *J. Eng. Mater. Technol. Transactions ASME*, 122(1):80–85, 2000.
- [14] G. Mishuris and A. Öchsner. 2D modelling of a thin elasto-plastic interphase between two different materials: Plane strain case. *Compos. Struct.*, 80(3):361–372, 2007.

- [15] D. Durban and P. Papanastasiou. Singular crack-tip fields for pressure sensitive plastic solids. *Int. J. Fract.*, 119(1):47–63, 2003.
- [16] G. Mishuris, W. Miszuris, A. Öchsner, and A. Piccolroaz. Transmission conditions for thin elasto-plastic pressure-dependent interphases. In H. Altenbach and A. Öchsner, editors, *Plasticity of Pressure-Sensitive Materials*, pages 205–251. Springer Berlin Heidelberg, Berlin, 2013.
- [17] W.F. Chen and D.J. Han. *Plasticity for structural engineers*. Springer-Verlag, New York, 1988.
- [18] V.A. Lubarda. Deformation theory of plasticity revisited. *Proc. Mont. Acad. Sci. Arts*, 13:117–143, 2000.